www.czasopisma.pan.pl PAN POLSKA AKADEMIA NAUK www.journals.pan.pl

Arch. Metall. Mater. **65** (2020), 4, 1303-1306

DOI: 10.24425/amm.2020.133689

KWANGMIN LEE[1*], SANGHYUN RHO[2]

PHASE TRANSITIONS AND ELECTROCHEMICAL CORROSION BEHAVIORS OF $Ti_{50}Ni_{50-x}Cu_x$ SHAPE MEMORY ALLOYS FOR METALLIC BIOMATERIALS

TiNi alloys have excellent shape memory properties and corrosion resistance as well as high biocompatibility. This study investigated the effects of copper addition on the phase transitions and electrochemical corrosion behaviors of $Ti_{50}Ni_{50-x}Cu_x$ alloys. TiNi, $Ti_{50}Ni_{47}Cu_3$, $Ti_{50}Ni_{44}Cu_6$, and $Ti_{50}Ni_{41}Cu_9$ alloys were prepared using vacuum arc remelting followed by 4 h homogenization at 950°C. Differential scanning calorimetry and X-ray diffraction analyses were conducted. The corrosion behaviors of the alloys were evaluated using potentiodynamic polarization test in Hank's balanced salt solution at a temperature of 36.5 ± 1°C. The TiNi alloy showed phase transitions from the cubic B2 phase to the monoclinic B19' phase when the alloy was thermally cycled. The addition of copper to the TiNi alloy played a major role in stabilizing the orthorhombic B19 phases during the phase transitions of $Ti_{50}Ni_{50-x}Cu_x$ alloys. The shifts in the corrosion potential toward the positive zone and the low corrosion current density were affected by the amount of Cu added. The corrosion resistance of the TiNi alloy increased with increasing copper content.

Keywords: $Ti_{50}Ni_{50-x}Cu_x$, Phase transition, Electrochemical corrosion behavior, DSC, PDP

1. Introduction

Nearly equiatomic Ti-Ni alloys have excellent shape memory properties and corrosion resistance as well as high biocompatibility [1]. Ti-Ni alloys have been extensively used in various medical devices, including endovascular stents, dental arch-wires, and orthopedic implants. Studies have found that the addition of a third alloying element, such as copper [2], iron [3], niobium [4], and zirconium [5], to Ti-Ni alloys leads to various phase transformations and imparts shape memory and other mechanical properties to Ti-Ni alloys.

The electrochemical behaviors of Ti-Ni alloys are of considerable interest because of their biological applications. Copper substitution is considered an elemental substitution that reduce the martensite transformation temperature, bringing it close to the temperature of human body [6]. Some research has focused on detailed phase transitions depending on the amount of copper [7,8]. By contrast, a few studies to date have presented a case in which local corrosion of a Ti-Ni-Cu alloy occurred in a NaCl solution [9]. Wen et al. unusually proposed that the addition of Cu had no influence on the corrosion potential and corrosion rate of $Ti_{50}Ni_{50-x}Cu_x$ alloy [10].

The present study investigated phase transitions and electrochemical corrosion behaviors of TiNi, $Ti_{50}Ni_{47}Cu_3$, $Ti_{50}Ni_{44}Cu_6$, and $Ti_{50}Ni_{41}Cu_9$ alloys using differential scanning calorimetry (DSC) and potentiodynamic polarization (PDP) tests.

2. Experimental

TiNi, $Ti_{50}Ni_{47}Cu_3$, $Ti_{50}Ni_{44}Cu_6$, and $Ti_{50}Ni_{41}Cu_9$ (at%) alloys were prepared through vacuum arc remelting at 1.5×10^{-3} Pa in an argon atmosphere. All specimens were homogenized at 900°C for 4 h, followed by a swaging process at 1000°C. Phase transformation temperatures of the alloys were measured using DSC (DSC-60, Shimadzu, Japan). The DSC procedure was conducted at heating and cooling rates of 10°C/ min. The specimens for the DSC were initially prepared with double thermal hysteresis from heating to 200°C, and then cooling to –50°C holding. The specimens were maintained for 5 min at each temperature. Crystal structures of the $Ti_{50}Ni_{50-x}Cu_x$ alloys were analyzed using a high-resolution X-ray diffractometer (X'Pert PRO Multipurpose X-Ray Diffractometer; PANalytical, Netherlands) equipped with a Cu Kα target. The electrochemical

[1] CHONNAM NATIONAL UNIVERSITY, SCHOOL OF MATERIALS SCIENCE & ENGINEERING, GWANGJU, REPUBLIC OF KOREA
[2] LG HAUSYS R&D CENTER, LG HAUSYS, SEOUL 07796, REPUBLIC OF KOREA
* Corresponding author: kmlee@jnu.ac.kr

experiments were conducted in a standard three-electrode cell corrosion tester (PARSTAT 2273, Princeton Applied Research, USA), which included a working electrode with an exposed area of 1 cm^2, a platinum mesh as a counter electrode, and a silver/silver chloride reference electrode. A corrosion test was conducted in physiological saline solution that included 0.9% NaCl with a pH of 7.14 at a temperature of 36.5 ± 1°C. A potentiodynamic curve was obtained from an open circuit following the stabilization operation. The corrosion curve was measured at a 1 mV/s scan rate under a potential condition of –1.5-2.0 V.

3. Results and discussion

Fig. 1 shows various DSC scans of $Ti_{50}Ni_{50-x}Cu_x$ alloys as a function of copper content and also includes phase transition temperatures for martensite transition start (M_s), martensite transition finish (M_f), austenite transition start (A_s), and austenite transition finish (A_f). The transition hysteresis on heating and cooling depends considerably on the alloy composition. Fig. 1(a) shows the transformation of TiNi characterized by a conversion from the monoclinic B19' phase to the cubic B2 phase upon heating and the reverse transformation upon cooling. Substantial differences in the DSC scans for $Ti_{50}Ni_{47}Cu_3$, $Ti_{50}Ni_{44}Cu_6$, and $Ti_{50}Ni_{41}Cu_9$ alloys are found in Figs. 1(b)-(d), which represent two-step phase transitions. The appearance of two peaks showed the formation of an orthorhombic B19 phase on heating and cooling. The orthorhombic B19 phase preceded the formation of the cubic B2 phase upon heating and the monoclinic B19' phase upon cooling. In addition, DSC scans of $Ti_{50}Ni_{44}Cu_6$ and $Ti_{50}Ni_{41}Cu_9$ alloys showed clear distinctions in the two-step phase transitions, as compared to the $Ti_{50}Ni_{47}Cu_3$ alloy. Wu and Chang recently reported a similar two-stage transformation of $Ti_{50}Ni_{40}Cu_{10}$ shape memory alloy [11]. Even though Nespoli et al. [12] proposed that B2→B19→B19' transformation originated starting from an addition of 8 at% of Cu, the present study found the two-step phase transitions when Cu content was 6 at% and showed distinct phase transitions in the DSC scans. Thus, the addition of copper played a major role in stabilizing the orthorhombic B19 phases during the phase transitions of $Ti_{50}Ni_{50-x}Cu_x$ alloys.

Table 1 shows summarized phase transition temperatures of the alloys obtained with the DSC scans shown in Fig. 1. The phase transition temperatures of the B19 and B2 phases upon heating and of the B19 and B19' phases upon cooling increased when the copper content increased. The phase transition temperatures of $Ti_{50}Ni_{50}$ corresponded to M_f = 38.0°C, M_s = 56.1°C, A_s = 60.0°C, and A_f = 84.5°C, whereas those of the $Ti_{50}Ni_{47}Cu_3$ alloy corresponded to M_f = –14.2°C, M_s = 7.1°C, A_s = 27.6°C, and A_f = 49.2°C. The transformation-induced deformation point (A_s) of $Ti_{50}Ni_{47}Cu_3$ showed the most suitable phase transition temperature, similar to the temperature of the human body, for metallic biomaterials.

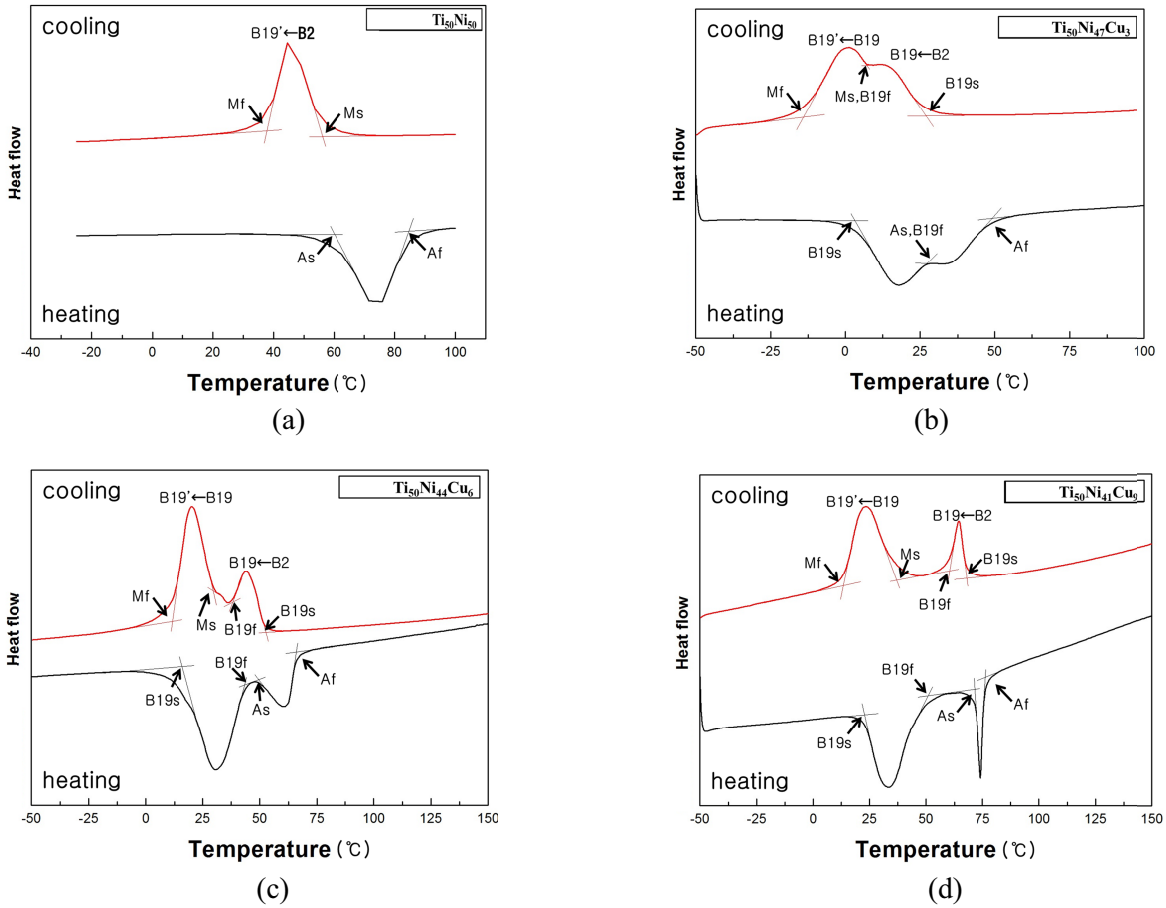

Fig. 1. DSC scans of $Ti_{50}Ni_{50-x}Cu_x$ alloys upon heating and cooling as a function of copper content

TABLE 1

Transformation temperatures of several $Ti_{50}Ni_{50-x}Cu_x$ alloys measured by DSC

(unit: °C)

	Heating				Cooling			
	$B19_s$	$B19_f$	A_s	A_f	$B19_s$	$B19_f$	M_s	M_f
TiNi	—	—	60.0	84.6	—	—	56.1	38.0
$Ti_{50}Ni_{47}Cu_3$	3.2	27.6	27.6	49.2	26.7	7.1	7.1	–14.2
$Ti_{50}Ni_{44}Cu_6$	15.9	43.6	49.4	65.9	52.6	39.4	29.9	11.6
$Ti_{50}Ni_{41}Cu_9$	23.0	51.1	71.5	76.7	67.9	60.0	36.9	13.6

Fig. 2 shows XRD data of $Ti_{50}Ni_{50-x}Cu_x$ alloys as a function of copper content. The peaks of cubic B2, orthorhombic B19, and monoclinic B19' phases were found in the specimens. As the amount of copper added to $Ti_{50}Ni_{50-x}Cu_x$ alloys increased, the peak intensities of the B19 and B19' phases also increased. Phase transformation of the cubic B2 to the monoclinic B19' phase with the formation of the B19 phase spontaneously occurred with high copper-content alloys, which was represented by typical phase transition sequences of B2→B19→B19' of the $Ti_{50}Ni_{50-x}Cu_x$ alloys, as discussed in the DSC results. The main peak intensity of the B19' phase on the (012) plane in the $Ti_{50}Ni_{41}Cu_9$ alloy was considerably higher than that of the B19 phase on the (020) plane.

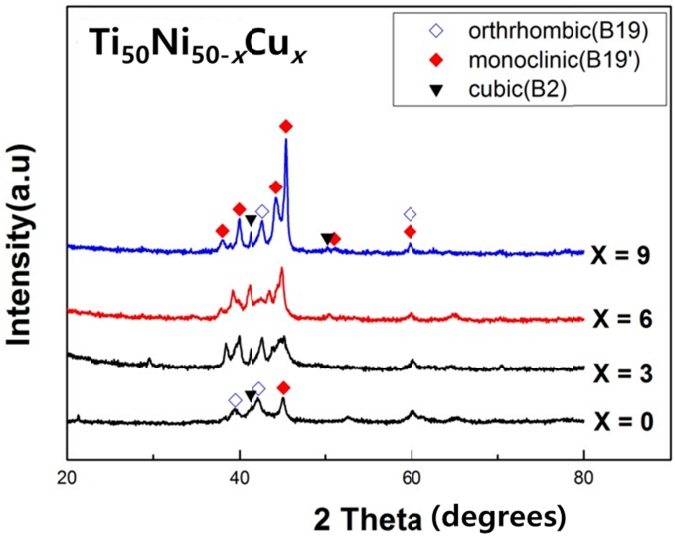

Fig. 2. X-ray diffraction pattern of $Ti_{50}Ni_{50-x}Cu_x$ alloys as a function of copper content

Fig. 3 shows the PDP curves of TiNi, $Ti_{50}Ni_{47}Cu_3$, $Ti_{50}Ni_{44}Cu_6$, and $Ti_{50}Ni_{41}Cu_9$ in a 0.9% NaCl solution at temperature of 36.5 ± 1°C. All specimens were spontaneously passivated upon anodic polarization. The passive current density of $Ti_{50}Ni_{47}Cu_3$ was found to be approximately 8.24×10^{-6} A/cm^2, which was slightly higher than that of the $Ti_{50}Ni_{44}Cu_6$, $Ti_{50}Ni_{41}Cu_9$ and TiNi. The highest passive current density for $Ti_{50}Ni_{47}Cu_3$ suggests that the alloying addition of 3% copper to TiNi could not significantly decrease the passive current density. By contrast, the alloying addition of 9% copper to TiNi caused a reduction in the passive current density (1.18×10^{-6} A/cm^2), which indicated the formation of more protective passive films. All alloys at anodic potentials greater than 0.75 V showed a significant increase in the current density because of oxygen evolution. An increase in the current densities suggested that the passive film formed on the surface had a lesser blocking effect in terms of electrolytic conductivity. Therefore, a higher current flow was allowed to oxidize the species in the electrolyte. The potential plateau observed after an abrupt increase in current densities corresponded to the secondary passivation on the surface. Considering a higher value of current densities at this potential plateau, the passive films in this region might be less stable and less protective as compared to those observed in the first passivation region that existed below the oxygen evolution region.

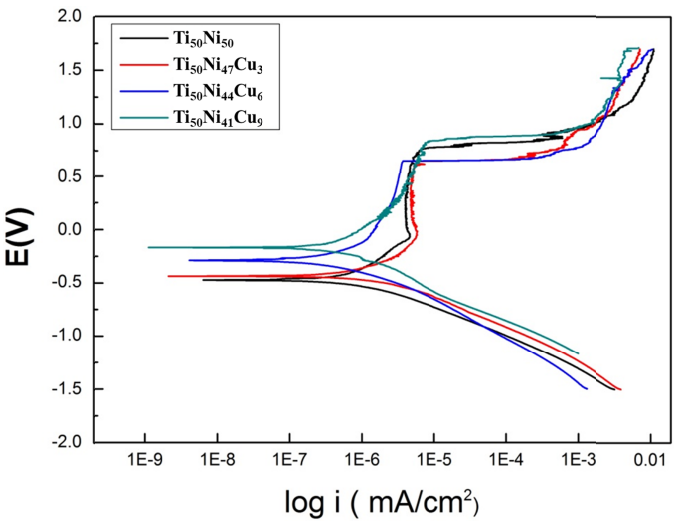

Fig. 3. PDP curves of $Ti_{50}Ni_{50-x}Cu_x$ alloys at a potential of 0.5 in a deaerated 0.9% NaCl solution at 36 ± 1°C

The corrosion parameters obtained with PDP scans are listed in Table 2. The values of the corrosion parameters corresponding to TiNi, $Ti_{50}Ni_{47}Cu_3$, $Ti_{50}Ni_{44}Cu_6$, and $Ti_{50}Ni_{41}Cu_9$ were not significantly different. $Ti_{50}Ni_{41}Cu_9$ exhibited a corrosion potential (E_{corr}) of –0.165 V, which was nobler than the corrosion potentials observed at TiNi, $Ti_{50}Ni_{47}Cu_3$, and $Ti_{50}Ni_{44}Cu_6$ with the values of –0.477, –0.439, and –0.287 V, respectively. However, Wen et al. reported opposing results in which the corrosion potential and corrosion rate of $Ti_{50}Ni_{50-x}Cu_x$ alloys were irrelevant to their Cu content, and the values were nearly the same as those of TiNi alloys [10]. The E_{corr} value of the TiNi alloy was

TABLE 2

Corrosion parameters obtained with PDP scans of $Ti_{50}Ni_{50-x}Cu_x$ alloys as a function of copper content

Alloys	E_{corr} (V)	I_{corr} (mA/cm^2)	Corrosion rate (cm/s)
TiNi	–0.477	7.66×10^{-7}	-2.66×10^{-13}
$Ti_{50}Ni_{47}Cu_3$	–0.439	1.33×10^{-6}	-4.18×10^{-13}
$Ti_{50}Ni_{44}Cu_6$	–0.287	1.85×10^{-7}	-2.49×10^{-14}
$Ti_{50}Ni_{41}Cu_9$	–0.165	2.19×10^{-7}	-3.72×10^{-14}

–0.477 V, which was lower than that of $Ti_{50}Ni_{50-x}Cu_x$ alloy. The values of corrosion current (i_{corr}) for $Ti_{50}Ni_{50-x}Cu_x$ were found to be of the order of 10^{-7}-10^{-8} A/cm^2. The corrosion rate of the $Ti_{50}Ni_{50-x}Cu_x$ alloy decreased with increasing Cu content. The lowest corrosion rate of 3.72×10^{-14} (cm/s) was obtained with the $Ti_{50}Ni_{41}Cu_9$ alloy.

4. Conclusion

The results of phase transitions and corrosion properties of $Ti_{50}Ni_{50-x}Cu_x$ alloys evaluated through DSC and corrosion test were as follows:

1. Thermal analysis determined the solid-solid transitions of $Ti_{50}Ni_{50-x}Cu_x$ alloys by measuring the hysteresis between the peak temperatures upon heating and cooling. The addition of copper to the TiNi alloy played a major role in stabilizing the orthorhombic B19 phases during the phase transitions of $Ti_{50}Ni_{50-x}Cu_x$ alloys. The transformation-induced deformation point (A_s) of $Ti_{50}Ni_{47}Cu_3$ showed the most suitable phase transition temperature, similar to the temperature of human body, for metallic biomaterials.
2. The $Ti_{50}Ni_{41}Cu_9$ alloy with E_{corr} of –0.165 V and the lowest corrosion rate of 3.72×10^{-14} (cm/s) showed outstanding corrosion resistance as compared to the $Ti_{50}Ni_{47}Cu_3$ and $Ti_{50}Ni_{44}Cu_6$ alloys. Increasing the alloying additions of Cu to TiNi alloys successfully suppressed the oxygen evolution, lowered the passive current density, and shifted the corrosion potential in the noble direction.

REFERENCES

[1] I. Yoshida, D. Monama, T. Ono, J. Alloy Compd. **448**, 349 (2008).
[2] T. Nam, J. Lee, D. Jung, C. Yu, Y. Liu, Y. Kim, Mater. Sci. Eng. **A 449**, 1041 (2007).
[3] S.K. Wu, H.C. Lin, T.Y. Lin, Mater. Sci. Eng. **A 438**, 536 (2006).
[4] X. He, L. Rong, D. Yan, Y. Lu, Scripta Mater. **53**, 1411 (2005).
[5] S. Inoue, N. Sawada, T. Namazu, Vacuum **83**, 664 (2009).
[6] A. Terayama, H. Kyogoku, Mater. Sci. Eng. **A 527**, 5484 (2010).
[7] Y. Tong, Y. Liu, Z. Xie, M. Zarinejad, Acta Mater. **56**, 1721 (2008).
[8] T. Nam, T. Saburi, K. Shimizu, Mater. Trans. JIM. **31**, 959 (1990).
[9] G. Rondelli, B. Vicentini, Biomater. **23**, 639 (2002).
[10] X. Wen, N. Zhang, X. Li, Z. Cao, Bio-Med. Mater. Eng. **7**, 1 (1997).
[11] S.K. Wu, Y.C. Chang, Mater. **12**, 2512 (2019).
[12] A. Nespoli, E. Villa, S. Besseghini, J. Alloy Compd. **509**, 644 (2011).